nature communications

Article

https://doi.org/10.1038/s41467-025-61801-2

Characterization of ferric hydroxysulfate on Mars and implications of the geochemical environment supporting its formation

Received: 22 January 2025

Accepted: 2 July 2025

Published online: 05 August 2025

Check for updates

J. L. Bishop[1,2], J. M. Meusburger[2], C. M. Weitz[3], M. Parente[4], C. Gross[5], D. Talla[6], A. M. Saranathan[4,7,8], Y. Itoh[4,9], M. R. D. Gruendler[1,10], A. E. G. Howells[2,11], M. Yeşilbaş[12], T. Hiroi[13], B. Schmitt[14], A. Maturilli[15], M. Al-Samir[5], T. F. Bristow[2], B. Lafuente[1,2] & M. Wildner[6]

Sulfate minerals are significant components of the martian surface and provide clues about the martian geochemical environment. One unusual Fe-sulfate phase has been intriguing Mars scientists for over a decade due to its unique spectral bands that are distinct from any known minerals and its occurrence in layered sedimentary rocks. We describe here detection of ferric hydroxysulfate ($Fe^{3+}SO_4OH$) and its implications for the geochemical history of Mars. Crystalline ferric hydroxysulfate is formed by heating hydrous Fe^{2+} sulfates to 100 °C or above and has a strong spectral band at 2.236 μm, similar to the spectral feature observed on Mars at Aram Chaos and on the plateau above Juventae Chasma. Hydrated sulfates at these locations likely formed through evaporative processes or low-temperature alteration. In contrast, $Fe^{3+}SO_4OH$ is more consistent with heating and oxidation of hydrated ferrous sulfates, potentially through deposition of lava, ash, or through hydrothermal processes.

The Compact Reconnaissance Imaging Spectrometer for Mars (CRISM) instrument in orbit at Mars has provided hyperspectral data for mapping numerous minerals that guide our understanding of the ancient geochemical history of Mars. A variety of sulfate minerals have been identified on Mars from orbital (e.g. refs. 1,2) and landed (e.g. refs. 3–5) missions through comparison with terrestrial minerals using spectral parameters, X-ray diffraction, and elemental abundances. An unusual spectral band at 2.236 μm was discovered in CRISM spectra of Mars at the plateau bordering Juventae Chasma[6] and in Aram Chaos[7] and has provided a challenge for mineral identification for over 15 years because this spectral band is not consistent with any known minerals. Preliminary lab investigations proposed dehydrated iron sulfates as the source of this unexplained material[6–8]. Recent advances in lab experiments on iron sulfates and improvements in the calibration of CRISM images are enabling identification and characterization of these intriguing martian outcrops, which we discuss in this study.

Results

Investigation of martian outcrops with unique ~ 2.23 μm spectral band

Characterizing these outcrops with unusual spectral signatures in CRISM images has benefitted from improved processing techniques[9]

[1]SETI Institute, Mountain View, CA, USA. [2]NASA Ames Research Center, Space Science and Astrobiology Division, Moffett Field, CA, USA. [3]Planetary Science Institute, Tucson, AZ, USA. [4]Department of Electrical and Computer Engineering, University of Massachusetts, Amherst, MA, USA. [5]Freie Universität Berlin, Institute of Geological Sciences, Berlin, Germany. [6]Department of Mineralogy and Crystallography, University of Vienna, Vienna, Austria. [7]Science Systems and Applications, Inc, Lanham, MD, USA. [8]NASA Goddard Space Flight Center, Greenbelt, MD, USA. [9]Johns Hopkins University Applied Physics Lab, Laurel, MD, USA. [10]University of California San Diego, La Jolla, CA, USA. [11]Blue Marble Space Institute of Science, Seattle, WA, USA. [12]Umeå University, Umeå, Sweden. [13]Department of Earth, Environmental and Planetary Sciences, Brown University, Providence, RI, USA. [14]University of Grenoble Alpes, CNRS, IPAG, Grenoble, France. [15]German Aerospace Center (DLR), Institute of Space Research, Berlin, Germany. e-mail: jbishop@seti.org

and mapping algorithms[10]. These remote sensing advances have uncovered previously unknown outcrops on Mars through analyses of smaller spot sizes with clearer spectra e.g. ref. 11. Analyses of CRISM images at the Juventae Plateau and Aram Chaos using these new techniques revealed additional outcrops of units containing this unique ~2.23 μm band along with other spectral features (Figs. 1 and 2). At the Juventae Plateau region, the outcrop containing the ~2.23 μm band is observed mixed with hydration bands similar to polyhydrated sulfates, and High Resolution Imaging Science Experiment (HiRISE) images show that thin units containing the 2.23 μm band occur primarily stratigraphically above the polyhydrated sulfate unit and in some cases also below the polyhydrated sulfate unit (Fig. 1, Supplementary Fig. S1, Supplementary data 1). Because these units are only 2-3 CRISM pixels wide in many cases (~40–50 m), spectra of the 2.23 μm band unit likely include a mixture of that phase and the polyhydrated sulfate unit below it. We analyzed the CRISM spectra of this 2.23 μm band material in comparison with lab spectra of hydrated sulfates and several species having bands somewhat near 2.23 μm. These include montmorillonite ($Na_{0.3}Al_2(Si_4O_{10})(OH)_2{\bullet}nH_2O$) with a band at 2.21 μm, nontronite ($Na_{0.3}Fe_2(Si_4O_{10})(OH)_2{\bullet}nH_2O$) with a band at 2.29 μm, gypsum ($CaSO_4{\bullet}2H_2O$) with a doublet at 2.22 and 2.26 μm, and jarosite ($KFe_3(SO_4)_2(OH)_6$) with a band at 2.26 μm and shoulders at 2.22 and ~2.3 μm. None of these minerals are consistent with the CRISM spectra of this outcrop having a single band near 2.23 μm. In addition to this enigmatic 2.23 μm band, this outcrop contains features near 1.43, 1.94, and 2.4 μm that are consistent with polyhydrated sulfates including rozenite ($FeSO_4{\bullet}4H_2O$) and epsomite ($MgSO_4{\bullet}7H_2O$) (Fig. 1d).

Outcrops containing a band near 2.23 μm in CRISM spectra are also observed at several locations at Aram Chaos. The units containing this unique spectral feature are mapped in red (Fig. 2, Supplementary Figs. S2, S3, and Supplementary data 1) and occur as small patches, but span several CRISM pixels, enabling improved isolation of the spectral properties of this material compared to the Juventae Plateau region. The 2.236 μm band is narrower in these spectra and is accompanied by additional sharp features at 1.48, 1.82, 2.19, and 2.37 μm that are attributed to ferric hydroxysulfate (Fig. 2). In Aram Chaos this 2.23 μm band material is most commonly observed adjacent to and beneath monohydrated sulfate outcrops mapped in green. Spectra of the monohydrated sulfate minerals szomolnokite ($FeSO_4{\bullet}H_2O$) and kieserite ($MgSO_4{\bullet}H_2O$) both have a band at 2.40 μm and another band near 2.1 μm that varies with composition. This band occurs at 2.09 μm in spectra of szomolnokite and at 2.13 μm in spectra of kieserite. Some of the monohydrated sulfate outcrops also include weak bands near 2.23 μm, indicating partial alteration to form a mixed phase containing some monohydrated sulfate and some $Fe^{3+}SO_4OH$ (Fig. 3). The polyhydrated sulfate spectra contain bands near 1.44 and 1.93-1.95 μm and a drop in reflectance near 2.42 μm (Fig. 3), similar to spectra of rozenite and starkeyite ($MgSO_4{\bullet}4H_2O$).

Formation of $Fe^{3+}SO_4OH$ in the lab

The potential mineral $Fe^{3+}SO_4OH$ is formed in the lab by heating dry powders of hydrated ferrous sulfates at temperatures from 100 to 300 °C[12,13]. Several $Fe^{3+}SO_4OH$ samples were produced in the lab (Table 1) and all include several narrow features due to vibrational bands, overtones, and combinations at 1.49, 1.83, 2.19, 2.236, 2.37, 2.61 and 2.89 μm. Additional Fe electronic absorptions produce a band near 0.94–0.96 μm that is broadened towards ~0.8 μm with a reflectance maximum near 0.7 μm, a drop in reflectance near 0.5 μm, and a narrow band at 0.43 μm, consistent with Fe^{3+} (Table 2, Fig. 3, Supplementary

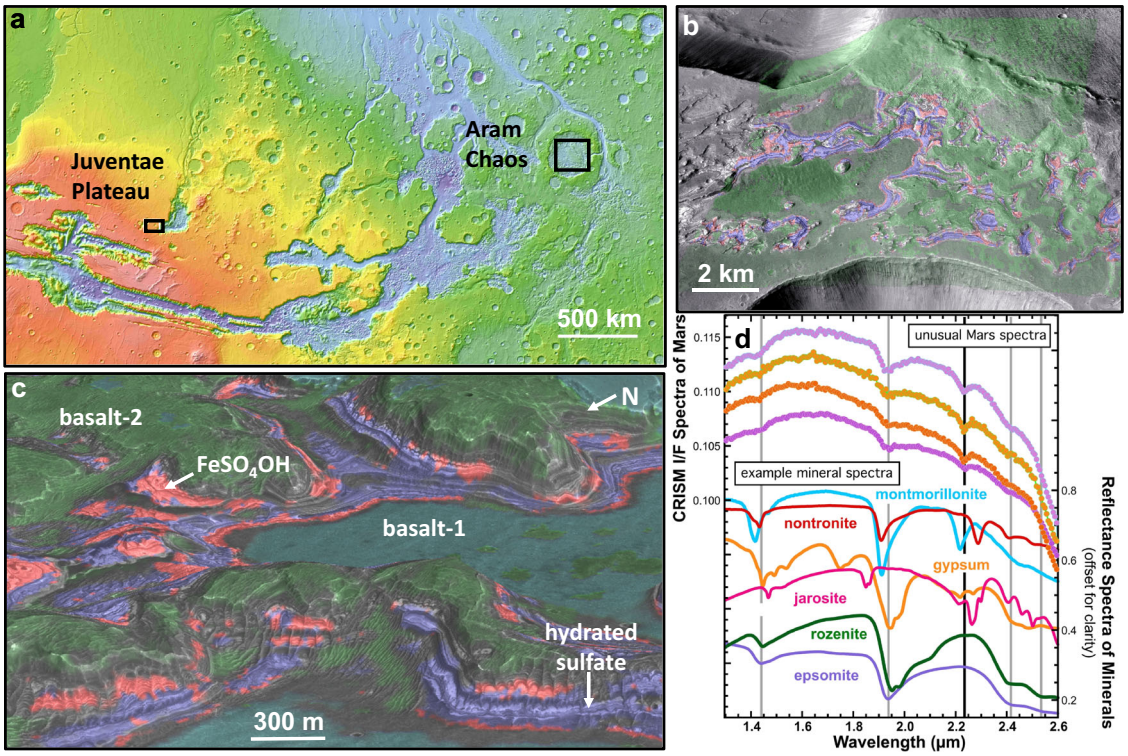

Fig. 1 | Spectrally distinct units at the Juventae Plateau. a Mars Orbital LASER Altimeter (MOLA) map of equatorial Mars with black boxes indicating locations of the Juventae Plateau and Aram Chaos (red indicates higher elevations and blue lower elevations). **b** View of the plateau above Juventae Chasma with compositional units from CRISM image FRT00005814 showing pyroxene-bearing basalt in green, polyhydrated sulfates in blue, and the $Fe^{3+}SO_4OH$-bearing phase in red over a High-Resolution Stereo Camera (HRSC) Digital Terrain Model (DTM). **c** Same CRISM compositional units over a HiRISE DTM (5x vertical exaggeration) with the basalt units split into basalt-1 in dark cyan and basalt-2 in medium green, scale bar for foreground. **d** CRISM spectra of unusual units with a band near 2.23 μm (top) and lab spectra of several minerals (bottom). Note that none of these minerals are a good spectral match to the CRISM spectra of the $Fe^{3+}SO_4OH$-bearing outcrop.

https://doi.org/10.1038/s41467-025-61801-2

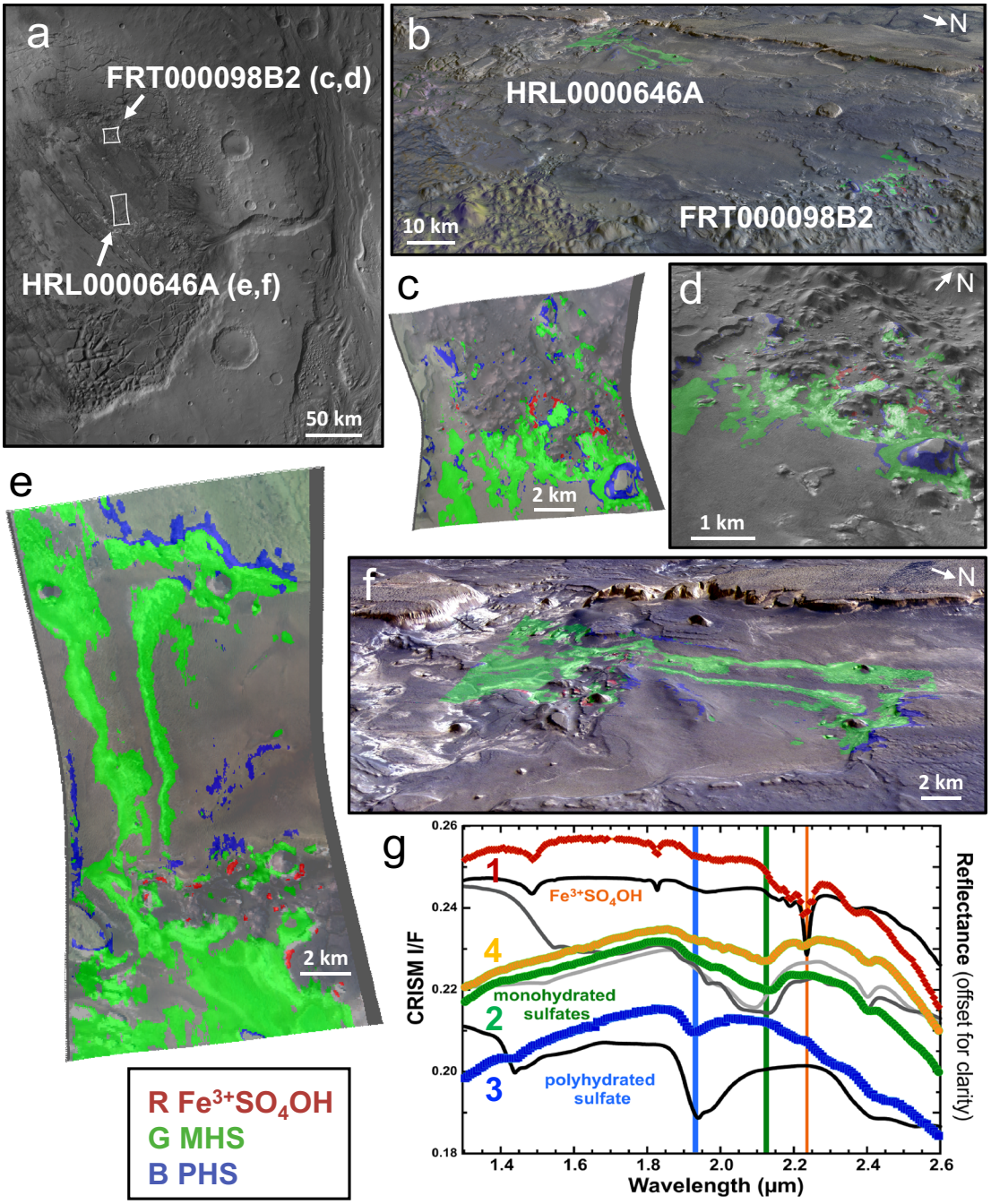

Fig. 2 | Spectrally distinct units at Aram Chaos. a HRSC view of Aram Chaos indicating locations of CRISM images. **b** Oblique view with CRISM mineral maps overlain on HRSC with red as $Fe^{3+}SO_4OH$, green as monohydrated sulfate (MHS), and blue as polyhydrated sulfate (PHS) (2x vertical). **c** Mineral map for CRISM image FRT000098B2. **d** Oblique view of CRISM image FRT000098B2 overlain on HRSC (2x vertical). **e** Mineral map for CRISM image HRL0000646A. **f** Oblique view of CRISM image HRL0000646A overlain on HRSC (2x vertical). **g** CRISM FRT000098B2 spectra compared with lab spectra of minerals: spectrum 1 (red diamonds) contains a strong 2.236 μm band, similar to lab spectra of $Fe^{3+}SO_4OH$ (black, top); spectrum 2 (green circles) has bands at 2.13 and 2.40 μm, consistent with kieserite ($MgSO_4{\bullet}H_2O$, dark gray, center); spectrum 3 (blue squares) is characteristic of PHS, similar to starkeyite ($MgSO_4{\bullet}4H_2O$, black, bottom); spectrum 4 (orange circles) has bands at 2.11, 2.225, and 2.40 μm and is attributed to a mixture of $Fe^{3+}SO_4OH$ and MHS (note – mapped as green in image due to dominant MHS features); szomolnokite ($Fe^{2+}SO_4H_2O$, light gray, center) spectrum shown for comparison.

data 2). These vibrational and electronic bands are distinct and readily distinguishable from the spectral properties of rozenite and szomolnokite e.g. refs. 6,14. Rozenite is characterized by Fe^{2+} bands near 0.98 and 1.18 μm with a reflectance maximum near 0.56 μm, while the Fe^{2+} band for szomolnokite occurs at ~0.94 μm with a broad reflectance maximum near 0.65–0.75 μm. The HOH stretching overtone occurs at 1.45 μm for rozenite and at 1.52 μm for szomolnokite, while the HOH stretch plus bend combination vibrations occur at 1.95 μm for rozenite and at 2.09 μm for szomolnokite. The H_2O vibrations observed for rozenite are similar to those observed for many types of polyhydrated sulfates, in contrast to the constrained H_2O sites for the monohydrated sulfates szomolnokite and kieserite that are shifted to longer wavelengths e.g. refs. 15,16. This difference in the position of the H_2O overtones and combination bands in hydrated sulfates enables clear discrimination of monohydrated versus polyhydrated sulfates on Mars[6]. Additional bands are observed for szomolnokite at 2.40 and

https://doi.org/10.1038/s41467-025-61801-2

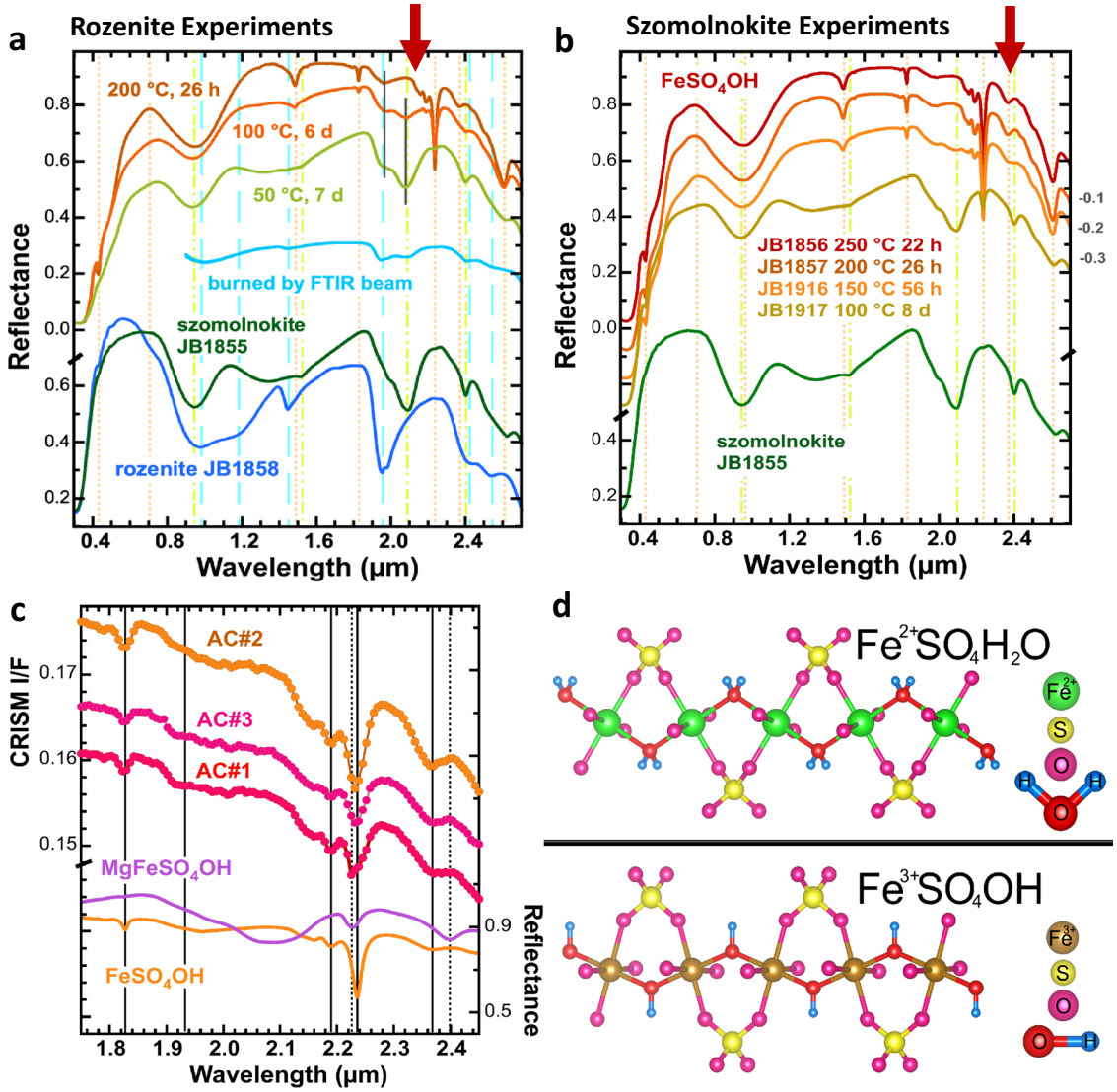

Fig. 3 | Properties of ferric hydroxysulfate. a VNIR reflectance spectra of products formed through heating rozenite, including $Fe^{3+}SO_4OH$ as well as mixtures of $Fe^{3+}SO_4OH$ with szomolnokite and mixtures of szomolnokite and rozenite. **b** VNIR reflectance spectra of products formed through heating szomolnokite, including $Fe^{3+}SO_4OH$ and mixtures of $Fe^{3+}SO_4OH$ with szomolnokite. **c** Comparison of lab spectra of $Fe^{3+}SO_4OH$ and $Mg^{2+}Fe^{3+}SO_4OH$ to CRISM spectra from Aram Chaos (Supplementary Fig. S3b); note that dots in the CRISM spectra represent individual CRISM datapoints. **d** Crystal structures of szomolnokite and ferric hydroxysulfate[17,21].

2.62 μm and for rozenite near 2.42 and 2.53 μm. The bands near 2.4 and 2.5 μm are often broadened in the spectra of polyhydrated sulfates such that only a drop in reflectance near 2.4 μm can be detected in remote sensing data.

Reflectance spectra of $Fe^{3+}SO_4OH$ were also measured under vacuum (Supplementary Fig. S4) and low-temperature (Supplementary Fig. S5) conditions to investigate changes in this potential new mineral under different environments more relevant to Mars. Overall, $Fe^{3+}SO_4OH$ appears stable under these conditions and only small shifts in a couple of bands were observed (Table 2). Additionally, the spectra measured under vacuum are very similar to those measured under controlled, dry conditions, thus providing confidence that purging the sample of H_2O overnight in the chamber before measurement adequately removes adsorbed water molecules.

A synthetic monohydrated sulfate with 50% Mg and 50% Fe^{2+} cations[17] was also heated for comparison with the $Fe^{3+}SO_4OH$ produced from heating szomolnokite and rozenite. This dehydrated $Mg_{0.5}Fe^{2+}_{0.5}$-MHS sample contains many bands similar to those of $Fe^{3+}SO_4OH$ (Table 2), but shifted slightly, as well as a band near 2.09 μm due to the unreacted $Mg_{0.5}Fe^{2+}_{0.5}$-MHS. Importantly, the OH combination band observed at 2.236 μm in spectra of $Fe^{3+}SO_4OH$, is shifted to 2.226 μm for $Fe^{3+}_{0.5}Mg^{2+}_{0.5}SO_4OH/H_2O$. Because the presence of Mg in this sample appears to have disrupted the deprotonation process, we characterized the reaction of szomolnokite to $Fe^{3+}SO_4OH$ further.

The $Fe^{3+}SO_4OH$ crystal structure includes octahedrally coordinated $Fe^{3+}O_6$ units with tetrahedrally coordinated SO_4 groups on opposite O atoms (~180 degrees apart) and bridging OH groups connecting the Fe^{3+} octahedra to form a linear configuration (Fig. 3c). This is similar to the structure of szomolnokite that has octahedrally coordinated Fe^{2+} instead of Fe^{3+} and two protons on bridging octahedral O atoms to form H_2O molecules instead of OH. Vibrations of these H_2O and OH groups in the structure of szomolnokite and $Fe^{3+}SO_4OH$, respectively, are responsible for the broad H_2O combination band near 2.1 μm and the narrow OH combination band at 2.236 μm. The structure of $Fe^{3+}SO_4OH$ and the strength of the bond connecting the OH group to the Fe^{3+} cation govern the vibrational energy of the OH group. The OH fundamental stretching vibration occurs at 3460 cm^{-1} or 2.89 μm (Table 2, Supplementary Fig S4). Jarosite also has OH groups bound to Fe^{3+} cations in an octahedral configuration, but the OH

Table 1 | Sample identification and descriptions

Sample ID	Name	Conditions	XRD
JB0626	Rozenite	From Iron Mountain[48]	Rozenite
JB0787	Copiapite	From RioTinto[6]	Copiapite
JB0788	Mixture copiapite, $FeSO_4OH$	Heated copiapite JB787 from 100 to 300 °C, unstable	mixture
JB1771	MHS with 50% Mg, 50% Fe^{2+}	Talla and Wildner[17]	Not measured; assumed similar to JB1874
JB1781	Szomolnokite	Talla and Wildner[17]	Not measured; assumed similar to JB1884
JB1782	$FeSO_4OH$	Heated rozenite JB626 from 50 to 300 °C	
JB1784	Mixture $MgFeSO_4OH/H_2O$, $FeSO_4OH$, and hydrated FeMg sulfate phases	Heated MHS 50%Fe/50%Mg JB1771 from 50 to 300 °C	Complex mixture; good fit obtained with 2x hydroxide, 2x mixed (Mg, Fe) phases and refining the lattice parameters.
JB1855	Szomolnokite	Synthesized at 60 °C	100% Szomolnokite
JB1856	$FeSO_4OH$	Heated JB1855 szomolnokite at 250 °C for 22 h	100% $FeSO_4OH$
JB1857	$FeSO_4OH$	Heated JB1855 szomolnokite at 200 °C for 26 h	100% $FeSO_4OH$
JB1858	Rozenite	Synthesized at 20 °C	100% rozenite
JB1859	$FeSO_4OH$	Heated JB1858 rozenite at 200 °C for 26 h	100% $FeSO_4OH$
JB1860	Fe sulfate mixture	Heated JB1858 rozenite at 100 °C for 5 days, 19 h	81% $FeSO_4OH$, 19% szomolnokite
JB1861	Szomolnokite	Synthesized at 60 °C	100% szomolnokite
JB1863	$FeSO_4OH$	Szomolnokite JB1861, heated 200 °C at DLR, 3.5 hrs	95% $FeSO_4OH$, 5% szomolnokite
JB1871	Mixture rozenite, szomolnokite	Rozenite heated at 50 °C for 7 days	90% szomolnokite, 10% rozenite
JB1874	MHS with 50% Mg, 50% Fe^{2+}	Talla and Wildner	100% mixed Mg-Fe^{2+}
JB1884	Szomolnokite	Talla and Wildner	93% szomolnokite, 7% rhomboclase
JB1916	Mixed szomolnokite - $FeSO_4OH$	Heated szomolnokite at 150 °C, 56 h	7% szomolnokite, 93% $FeSO_4OH$
JB1917	Mixed szomolnokite - $FeSO_4OH$	Heated szomolnokite at 100 °C, 8 days	73% szomolnokite, 27% $FeSO_4OH$
JB1918	Mixed rozenite - szomolnokite	Burned JB1858 rozenite sample surface with FTIR beam	5.5% szomolnokite, 94.5% rozenite
JB1919	Mixed szomolnokite - $FeSO_4OH$	Heated szomolnokite at 100 °C, 19 days	62% szomolnokite, 38% $FeSO_4OH$
JB1920	Butlerite	$FeSO_4OH$ rehydration for 1 week at 70% RH and room temperature	Nearly phase pure butlerite; two unindexed impurity peaks with <1% of maximum intensity.

All mineral abundancies in weight %; all ferric hydroxysulfate assumed to contain Fe^{3+} cations; all rozenite and szomolnokite assumed to have Fe^{2+} cations.

stretching vibrations occur near 3385 cm^{-1} or 2.95 μm for K^+-jarosite and 3360 cm^{-1} or 2.98 μm for Na^+-jarosite[18]. Presumably, the additional Na^+ or K^+ cations in the jarosite structure are pulling some of the electron density away from the OH bond, thus reducing the vibrational energy and shifting the bands towards longer wavelengths compared to the OH vibrations in ferric hydroxysulfate. In contrast, the rozenite crystal structure[19] (Supplementary Fig. S6) forms isolated clusters of two $Fe^{2+}O_6$ octahedra linked to two SO_4 tetrahedra via O atoms that are ~90 degrees apart in the Fe^{2+} octahedron. For rozenite, the O atoms not connected to sulfate groups are each bound to two protons to form four H_2O molecules per $Fe^{2+}O_6$ octahedron. The colors of the <125 μm grain size powders of these iron sulfates are very pale green for rozenite, white for szomolnokite, and orange for $Fe^{3+}SO_4OH$ (Supplementary Fig. S7). Sample JB1917 contains 27 wt.% $Fe^{3+}SO_4OH$ and 73 wt.% szomolnokite and is a light tan color (Supplementary Fig. S7). Samples with larger grain sizes have deeper colors (not shown).

Experiments heating szomolnokite, rozenite, melanterite ($Fe^{2+}SO_4{\bullet}7H_2O$), and copiapite ($Fe^{2+}Fe^{3+}{}_4(SO_4)_6(OH)_2{\bullet}20H_2O$) in ambient conditions in the lab resulted in production of $Fe^{3+}SO_4OH$ at elevated temperatures[6–8,13,20]. $Fe^{3+}SO_4OH$ was produced by heating rozenite or szomolnokite at 200 °C for 26 h (Table 1) or melanterite to 240 °C for 18 h[7]. Rozenite heated at 30 min intervals at 50 °C, 100 °C, then 150 °C produced some $Fe^{3+}SO_4OH$ and continued heating at 50 °C intervals to 300 °C resulted in strong $Fe^{3+}SO_4OH$ spectral signatures (Supplementary Fig. S8). In contrast, interval heating of copiapite produced some $Fe^{3+}SO_4OH$ by 200 °C and more $Fe^{3+}SO_4OH$ by 300 °C, and interval heating of szomolnokite did not result in formation of $Fe^{3+}SO_4OH$ until 300 °C (Supplementary Fig. S8). Reaction of poly-hydrated sulfates at lower temperatures than szomolnokite suggests that H_2O facilitates the transformation to $Fe^{3+}SO_4OH$.

Slower reaction kinetics were evident at lower temperatures in a series of experiments with rozenite and szomolnokite (see Table 1 for a summary of all Fe sulfate reactions). Szomolnokite heated at 150 °C for 56 hours produced 93 wt.% $Fe^{3+}SO_4OH$. Rozenite heated at 100 °C for 6 days resulted in 81 wt.% $Fe^{3+}SO_4OH$, but only 27 wt.% $Fe^{3+}SO_4OH$ resulted after 8 days starting from szomolnokite. Heating of rozenite at 50 °C resulted in dehydration of ~90% of the sample to szomolnokite after 7 days and heating of the rozenite sample by the FTIR beam in wide aperture mode resulted in partial formation of szomolnokite at the surface. No evidence of $Fe^{3+}SO_4OH$ was observed for these lower temperature reactions.

Additional heating experiments of szomolnokite in sealed vials containing nitrogen gas or air demonstrated that oxygen is required for reaction of these hydrated ferrous sulfates to form ferric hydroxysulfate[13] (Supplementary S1/Supplementary Table 1). Gas pressures were recorded at the beginning and end of each experiment. Initial gas pressures ranged from 1.29 to 1.36 bars and were decreased in the reactions where O_2 was consumed and $Fe^{3+}SO_4OH$ was formed. Characterization of the solid phase by X-ray diffraction and the gas phase by gas chromatography before and after the heating experiment

https://doi.org/10.1038/s41467-025-61801-2

Table 2 | Ferric hydroxysulfate spectral bands

Sample ID	Sample description	Wavelengths of spectral bands in μm										
Measured at RELAB, Brown University, under controlled dry conditions												
JB1856	Heated szomolnokite 250 °C	0.430	0.955	1.488	1.827	1.966		2.191	2.236	2.369	2.609	2.887
JB1857	Heated szomolnokite 200 °C	0.430	0.955	1.486	1.827	1.966		2.191	2.236	2.369	2.608	2.884
JB1859	Heated rozenite 200 °C	0.430	0.940	1.486	1.827	1.962		2.191	2.236	2.369	2.607	2.885
JB1784	Heated $Mg_{0.5}Fe_{0.5}$-MHS 300 °C	0.425	0.935	1.526	1.822	2.087		2.090	2.228	2.399	2.609	2.882
Measured under vacuum at PSL, DLR-Berlin												
JB1856	initial			1.487	1.827	1.969	1.987	2.190	2.236	2.367	2.609	2.884
JB1856	after 15 minutes			1.486	1.827	1.971	1.987	2.190	2.236	2.367	2.609	2.884
JB1856	after 30 minutes			1.486	1.827	1.974	1.987	2.190	2.236	2.367	2.609	2.884
Measured under vacuum and decreasing temperatures at IPAG, University of Grenoble												
JB1856	293 K	0.43	0.95	1.49	1.825	1.96		2.19	2.235	2.37	2.605	2.89
JB1856	273 K	0.43	0.96	1.49	1.825	1.97		2.19	2.235	2.37	2.605	2.89
JB1856	243 K	0.43	0.96	1.49	1.825	1.97		2.19	2.235	2.37	2.605	2.89
JB1856	213 K	0.43	0.97	1.49	1.825	1.97		2.19	2.235	2.37	2.605	2.89
JB1856	189 K	0.43	0.97	1.49	1.825	1.97		2.19	2.235	2.37	2.605	2.89

indicates that the formation of $Fe^{3+}SO_4OH$ proceeds via the reaction in Eq. (1).

$$4\,Fe^{2+}SO_4 \cdot H_2O + O_2 \rightarrow 4\,Fe^{3+}SO_4OH + 2H_2O \quad (1)$$

Rietveld refinement supports formation of *C*2/*c* monoclinic $Fe^{3+}SO_4OH$ (Fig. 4, Supplementary Fig. S9). Comparison of the crystal structures of $Fe^{3+}SO_4OH$ and szomolnokite[17,21] suggests that the transformation is associated with a loss of a hydrogen atom bonded to the bridging oxygen likely occurring coincidently with the oxidation of Fe^{2+} to Fe^{3+}. The structure remains largely intact throughout the transformation; however, the polyhedral units rotate and distort to accommodate the changes in charge distribution (Fig. 3c), where the increased charge on the Fe atom is compensated by the negative charge on the hydroxyl group. Heating experiments with kieserite were not successful in creating a stable hydroxide phase, likely because Mg does not exist in trivalent form. This is also reflected in the mixed cation monohydrated sulfate samples heated at 300 °C that only showed incomplete transformation to the hydroxide phase.

Morphologies of ferric hydroxysulfate and associated units

Evaluating the morphologies and stratigraphies of the sulfate outcrops at the Juventae Plateau and Aram Chaos enables the determination of relationships among the different sulfate units. Spectra at the Juventae Plateau were collected from ~30 to 35 m thick light-toned layered deposits that exhibit spectral signatures consistent with polyhydrated sulfates and $Fe^{3+}SO_4OH$, plus pyroxene-bearing units (Figs. 1 and 5, Supplementary Fig. S1). Thin units containing spectral features consistent with polyhydrated sulfates and $Fe^{3+}SO_4OH$ are mapped in blue and red, respectively (Figs. 1 and 5). The stratigraphy of the outcrops shows a pyroxene-bearing substrate below the light-toned layered materials termed basalt-1 (dark cyan) and a different pyroxene-bearing caprock unit covering the Fe sulfates termed basalt-2 (medium green) (Supplementary Fig. S1). CRISM spectra of the basalt-1 material include spectral properties most similar to augite (high-Ca pyroxene) with a reflectance maximum near 1.65 μm and a band centered near 2.35 μm, while the basalt-2 spectra likely contain some pigeonite (pyroxene enriched in Mg and Fe) due to shifts in the reflectance maximum and the ~2 μm band towards shorter wavelengths. Morphologies of these primary four units indicate that the pyroxene bearing substrate (dark cyan in both CRISM and HiRISE color) is flatter and appears clean (i.e., minimal dust and sand) with extensive polygonal fracturing, whereas the pyroxene-bearing caprock (medium green in CRISM and brown in HiRISE color) is partially composed of linear aeolian ripples and appears hilly and uneven in topography due to differential erosion. The textures of the polyhydrated sulfate and $Fe^{3+}SO_4OH$/polyhydrated sulfate units are distinct from those of the pyroxene-bearing units, but appear similar to each other with fine-scale layering that varies in brightness, color, and fracturing. The $Fe^{3+}SO_4OH$ unit is observed overlying the polyhydrated sulfate units in the stratigraphy and in some cases it is also present along the base of the light-toned materials as well. Thus, there may have been two different times when the $Fe^{3+}SO_4OH$ unit formed.

At Aram Chaos, monohydrated sulfates are the most abundant sulfate in the two CRISM images where $Fe^{3+}SO_4OH$ is present and are mapped in green (Figs. 2 and 6). The monohydrated sulfate units also exhibit variability in the band near 2.1 μm and are consistent with mixtures of szomolnokite and kieserite in some locations and of pure kieserite in other locations (Fig. 6, Supplementary Figs. S2, S3). Several patches of $Fe^{3+}SO_4OH$ are observed adjacent to and beneath the monohydrated sulfate outcrops, with some closer to kieserite-type outcrops and others next to mixed monohydrated sulfate outcrops. Variations are also observed in the polyhydrated sulfate units that are mapped in blue, with some outcrops exhibiting stronger hydration signatures. The stratigraphy indicates that polyhydrated sulfate units are observed at higher elevations than the monohydrated sulfates and $Fe^{3+}SO_4OH$ units, and in some cases pyroxene-bearing basalt is observed below the sulfates within the chaos blocks, although it is much rarer than the basalt units at the Juventae Plateau.

The $Fe^{3+}SO_4OH$ unit occurs along the floor of Aram Chaos and is stratigraphically the lowest sulfate unit relative to the monohydrated and polyhydrated sulfates. The $Fe^{3+}SO_4OH$ unit is medium-toned in brightness and exhibits polygonal fracturing and ridges, which can be either circular or linear, compared to the much brighter and scalloped fracturing observed in the monohydrated sulfate units. The monohydrated sulfate units can also be more jagged and hilly compared to the flatter and subdued morphology of the $Fe^{3+}SO_4OH$ unit. The only difference in morphology between the kieserite-type outcrops and the szomolnokite-kieserite outcrops is that the kieserite-type outcrops are slightly darker and appear mantled by loose debris and aeolian ripples. The polyhydrated sulfate unit is generally medium-toned in brightness relative to the other sulfates, which may be due to the widespread ripples and debris covering its surface. The unit is relatively flat, forming broad plateaus, but steeper cliffs along specific layers within the polyhydrated sulfate unit correspond to bright-toned, heavily fractured, and jagged outcrops. The morphology of the $Fe^{3+}SO_4OH$ and polyhydrated sulfate units are much easier to distinguish at Aram Chaos relative to the same units at Juventae Chasma.

https://doi.org/10.1038/s41467-025-61801-2

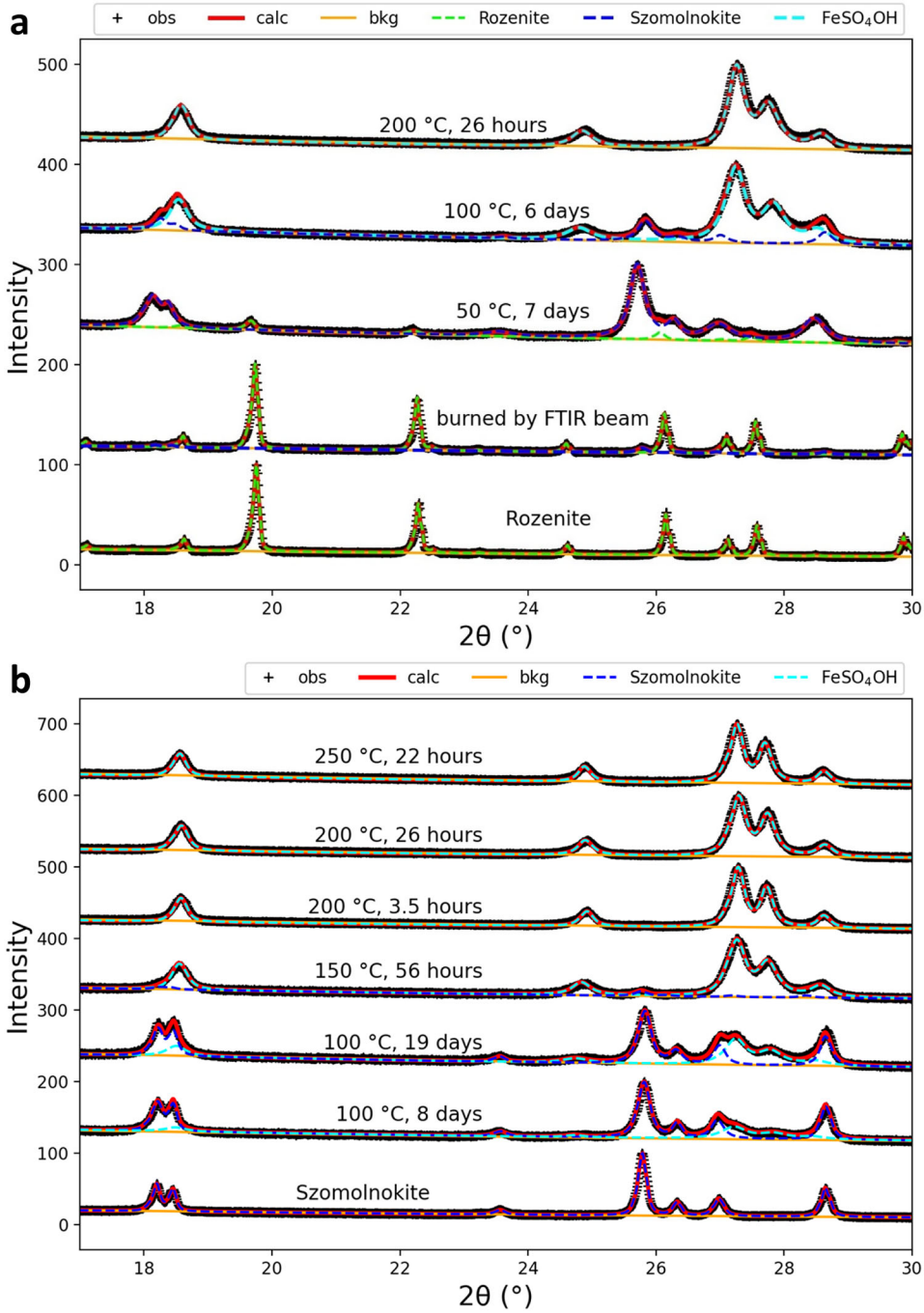

Fig. 4 | Rietveld refinements of the heating products of ferrous sulfates. a Rozenite. **b** Szomolnokite. Black lines with markers are the measured data, red solid lines are the overall fit, and dashed lines are contributions of each of the individual mineral phases to the overall fit.

Discussion

Exposures of this unusual iron sulfate phase with spectral features at 2.236 μm at Aram Chaos closely resemble pure $Fe^{3+}SO_4OH$ formed in the lab, whereas the thinner units on the Juventae Plateau are either mixed with other components or represent incompletely formed $Fe^{3+}SO_4OH$ phases. This ferric hydroxysulfate is currently associated with monohydrated sulfate outcrops at Aram Chaos, although polyhydrated sulfate outcrops are also present nearby. In contrast, primarily polyhydrated sulfate outcrops are currently observed on the Juventae Plateau.

Small variations in the ~2.23 μm band are attributed to changes in the Fe-Mg chemistry. Although the majority of spectra have a band centered at 2.236 μm, some exhibit a band centered at 2.225 μm instead (Supplementary Figs. S2, S3, Supplementary data 1, 2). Pure $Fe^{3+}SO_4OH$ has a band at 2.236 μm, while heated FeMg- monohydrated sulfate has a band at 2.226 μm. The $Fe^{3+}SO_4OH$ units at Aram Chaos are typically found adjacent to and beneath monohydrated sulfate outcrops (Fig. 2), including both Fe-rich monohydrated sulfate (similar to szomolnokite) with bands near 2.11–2.12 and 2.40 μm and kieserite ($MgSO_4{\bullet}H_2O$) with spectral bands near 2.13 and 2.41 μm. However, spectra of szomolnokite and kieserite measured at colder, Mars-like temperatures have bands at ~2.11 and 2.14 μm, respectively[22], similar to these observations. The monohydrated sulfate spectral units more consistent with kieserite are darker than the szomolnokite-like monohydrated sulfate units and are covered by debris and ripples (Figs. 2c and 5d, e). Some of the monohydrated sulfate units at Aram

https://doi.org/10.1038/s41467-025-61801-2

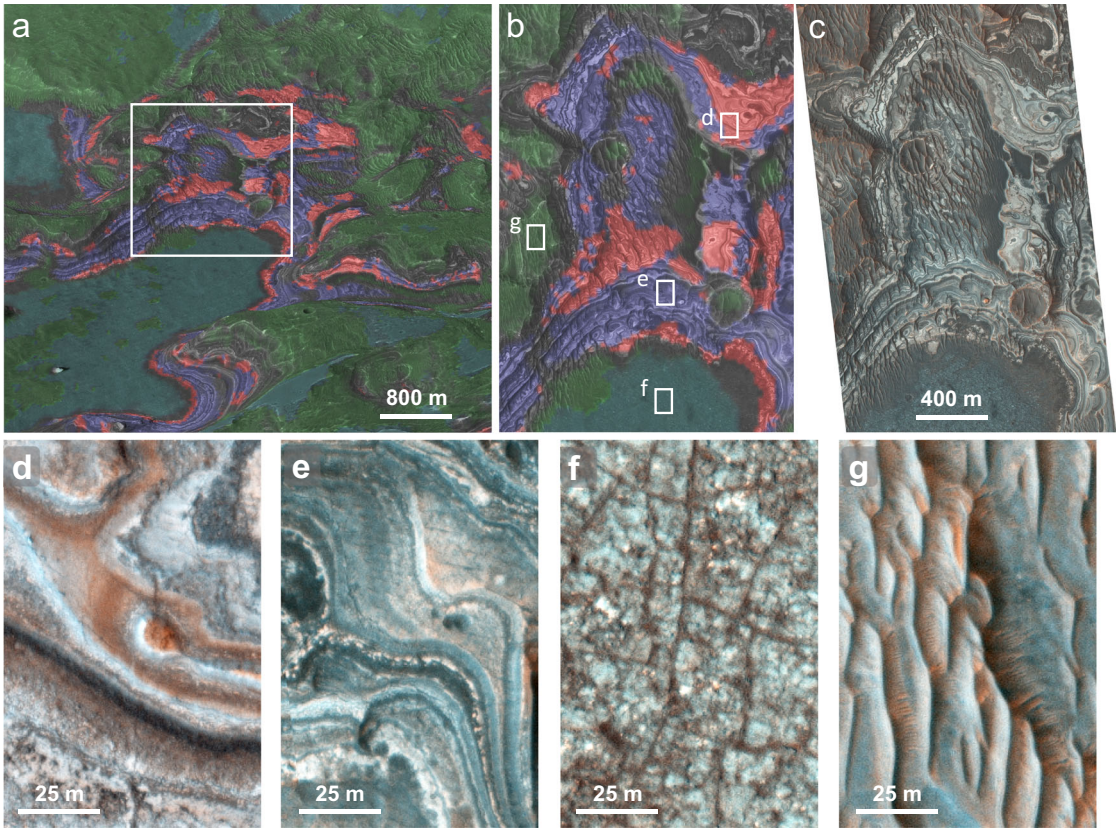

Fig. 5 | Morphologies of Geologic Units on the Juventae Plateau. a Mineral map from CRISM image FRT00005814 overlain on HiRISE DTM with red assigned to the $Fe^{3+}SO_4OH$-bearing phase, blue to polyhydrated sulfate, dark cyan to pyroxene-bearing basalt-1, and medium green to pyroxene-bearing basalt-2. **b** View of zoomed in region from white box in (**a**). **c** View of enhanced color HiRISE image for same region shown in (**b**). **d**–**g** HiRISE enhanced color blowups. **d** Morphology of $Fe^{3+}SO_4OH$-bearing unit. **e** Morphology of polyhydrated sulfate unit. **f** Morphology of pyroxene/basalt-1 unit. **g** Morphology of pyroxene/basalt-2 unit.

Chaos may have formerly been mixtures of szomolnokite and kieserite, where the szomolnokite transformed to $FeSO_4OH$ and the kieserite remained. Alternatively, polyhydrated Fe and Mg sulfates may have been present that were altered to form $Fe^{3+}SO_4OH$, szomolnokite, and kieserite, depending on variations in the geochemistry and temperatures.

The presence of pure $Fe^{3+}SO_4OH$ outcrops adjacent to monohydrated sulfate at Aram Chaos and less pure outcrops of $Fe^{3+}SO_4OH$ next to and mixed with polyhydrated sulfate on the plateau NW of Juventae Chasma indicate an active geochemical history in Mars' past (Fig. 7). The hydrated sulfates may have formed in sulfate brine environments and could have formed in cold or moderate waters, but the $Fe^{3+}SO_4OH$ materials would have required elevated temperatures to form. The $Fe^{3+}SO_4OH$-bearing units at the Juventae Plateau are mixed with polyhydrated sulfate at the scale of CRISM measurements (18 m/pixel) and could also be mixed with spectrally neutral components (altered ash) that dilute the $Fe^{3+}SO_4OH$ spectral features. Interestingly, light-toned layered deposits, sinuous landforms, and inverted channels exist across a wider area on the Juventae Plateau[23,24]. However, the sulfates are only observed in the smaller region of the plateau at a slightly lower elevation, located between the two chasma walls that drop steeply in elevation (Supplementary Fig. S10). Sulfates may exist in other regions of the plateau below the detection limits of CRISM or below the caprock. The inverted channels and drainage features indicate fluvial activity on the Juventae Plateau that could have been associated with the sulfates. Darker regions in THEMIS nighttime images (Supplementary Fig. S10b) represent lower thermal inertia, indicating highly porous, fine-grained materials[25]. These features are consistent with deposition of altered material at the lowest elevation where the sulfates are located. Additional blended CRISM-HiRISE views illustrate the stratigraphy of the sulfate units sandwiched in between the upper basalt-2 and lower basalt-1 units (Fig. 8).

Models of formation mechanisms of the two different forms of the $Fe^{3+}SO_4OH$ outcrops observed at the two different locations studied here (Fig. 7) illustrate potential pathways that could have taken place on Mars. At the Juventae Plateau, formation or deposition of polyhydrated sulfates occurred on top of basaltic material that was likely derived from volcanic ash or lava. The sulfates could have formed through alteration of volcanic ash in S-rich brines. Later emplacement of a different basaltic material (basalt-2) on top of the sulfates likely covered the area. Heat from this upper basalt-2 unit, assuming it was a hot volcanic flow or ash, could then have induced reaction of the hydrous Fe^{2+} sulfates to partially alter to $Fe^{3+}SO_4OH$ at spatial scales of ~20–50 m observed in the upper $Fe^{3+}SO_4OH$ unit. The majority of the $Fe^{3+}SO_4OH$/polyhydrated sulfate unit lies stratigraphically above the polyhydrated sulfate unit, indicating the hot upper basalt-2 unit could have been the heat source for reaction of the polyhydrated sulfate. The basal $Fe^{3+}SO_4OH$ unit observed in some locations may have formed through geothermal heating or still warm lavas of the basalt-1 unit. Because only weak traces of monohydrated sulfate features are observed, temperatures were likely higher, perhaps over 200 °C. Wind erosion removed portions of the upper basalt-2 unit over time exposing the $Fe^{3+}SO_4OH$/polyhydrated sulfate, polyhydrated sulfate, and basalt-1 units below. Small amounts of the $FeSO_4OH$/polyhydrated sulfate material may have mass wasted down to borders of the polyhydrated sulfate and basalt-1 units in certain areas, or some of the polyhydrated sulfate unit may have been altered by a geothermal source below this site. Light-toned layered deposits are associated with inverted channels, valley formations, and sulfate-bearing outcrops in or near many of the chasma surrounding Valles

https://doi.org/10.1038/s41467-025-61801-2

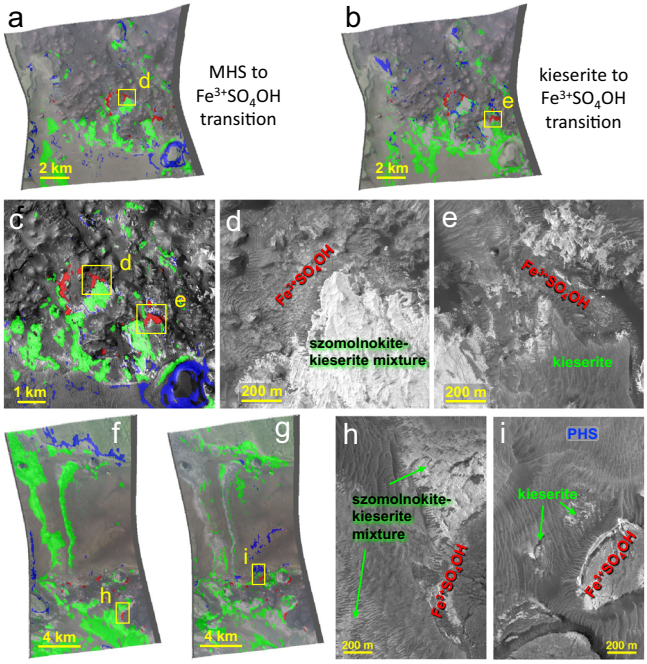

Fig. 6 | Morphologies of sulfate units at Aram Chaos. a Mineral map from CRISM image FRT000098B2 over MOLA with red assigned to the ~2.23 μm phase, blue to PHS-1, and green to MHS-1. **b** Mineral map from CRISM image FRT000098B2 with red assigned to the ~2.23 μm phase, blue to PHS-2, and green to MHS-2 (kieserite). **c** CRISM mineral map from (**a**) overlain on two HiRISE images with yellow boxes marking locations of views in (**d**, **e**). **d** Morphology of $Fe^{3+}SO_4OH$ and MHS-1 units. **e** Morphology of $Fe^{3+}SO_4OH$ and MHS-2 (kieserite) units. **f** Mineral map from CRISM image HRL0000646A with red assigned to the ~2.23 μm phase, blue to PHS-1, and green to MHS-1. **g** Mineral map from CRISM image HRL0000646A with red assigned to the ~2.23 μm phase, blue to PHS-2, and green to MHS-2 (kieserite). **h** Morphologies of $Fe^{3+}SO_4OH$ and MHS-1 units. **i** Morphologies of $Fe^{3+}SO_4OH$, MHS-2 (kieserite), and PHS units.

Marineris[26] and could include additional locations where ferric hydroxysulfate might be present.

At Aram Chaos the $Fe^{3+}SO_4OH$ unit is observed at the base of the hydrated sulfates, just above the bedrock (Fig. 6) as noted previously[7]. The chaos bedrock materials in this region likely formed through melting of subsurface ice or drainage of subsurface waters that produced catastrophic groundwater outflow and associated surface collapse e.g. ref. 27, about 3 Ga[28]. Subsequent aqueous activity produced the layered sedimentary material[29], later identified as sulfates[7]. These hydrated sulfates are proposed to have formed through multiple wetting events including groundwater recharge and evaporation[7]. Finally, hydrothermal activity at this site could have been responsible for heating of the polyhydrated sulfate materials to form the monohydrated sulfate and $Fe^{3+}SO_4OH$ units (Fig. 7). The observation of ferric hydroxysulfate in some regions of Aram Chaos, primarily surrounded by and beneath monohydrated sulfate, that are partially covered by polyhydrated sulfates is consistent with heating from below, and a geothermal hot spot at Aram Chaos could have been responsible for formation of the sulfate outcrops observed today. Geothermal activity in the chaos region may have also been responsible for formation of its morphology, e.g. ref. 30.

Determining a temperature for these hydrothermal sulfate reactions is difficult given the potential for long geologic timescales. Lab heating experiments at 100 °C observed slow formation of $Fe^{3+}SO_4OH$ from powders of both rozenite and szomolnokite, although the reactions proceeded faster from rozenite. This is presumably because of the additional H_2O molecules present in the rozenite structure that facilitate the reaction. Lab experiments heating rozenite at 50 °C did not produce $Fe^{3+}SO_4OH$ after several days. Additionally, szomolnokite crystals synthesized over 35 years ago[31] and stored at room temperature in Earth's oxygen-rich atmosphere remain well preserved, suggesting that the transformation to $Fe^{3+}SO_4OH$ does not occur under present-day martian atmospheric conditions, which are both oxygen-poor and low in temperature. Precipitation of $Fe^{3+}SO_4OH$ was found to occur via slow formation from a saturated aqueous iron sulfate solution at 120 °C after several weeks[32], but was not observed to form in highly concentrated sulfuric acid solutions at temperatures up to 210 °C[17]. The reason for this is likely that $Fe^{3+}SO_4OH$ is not a dehydrated form of szomolnokite, but rather it is formed via coordinated deprotonation and oxidation reactions. Thus, aqueous precipitation of $Fe^{3+}SO_4OH$ is not expected at low temperatures and is only sluggish at elevated temperatures. Further, it would be difficult to explain the observed stratigraphy of sulfates at Aram Chaos if $Fe^{3+}SO_4OH$ had formed via aqueous precipitation. Together, this reasoning suggests that the hydrothermal event at Aram Chaos that formed $Fe^{3+}SO_4OH$ reached temperatures above 50 °C. The largest support for our formation model at Aram Chaos, based on the burial and subsequent exhumation of Fe^{2+} sulfate hydrates, is the stratigraphic context of the $Fe^{3+}SO_4OH$ phase observed from orbit. Potentially, long-term heating of rozenite on Mars could have occurred at lower temperatures to form the szomolnokite and then shorter-term hydrothermal events produced the $Fe^{3+}SO_4OH$ phase. Wind erosion at Aram Chaos produced wide corridors where the bright sulfate-rich materials were removed[33]. The ~2.23 μm spectral feature is only observed in sites where erosion was sufficiently significant to expose the lowermost chaos floor[7].

Sulfate outcrops including associated polyhydrated sulfate and monohydrated sulfate units are common throughout the greater Valles Marineris region[1] and the ~3 Ga chaotic terrains associated with outflows from Chryse Basin[34,35]. The hydrated sulfates at Aram Chaos and the Juventae Plateau must have formed after these chaotic terrains and the ferric hydroxysulfate would have formed even more recently, perhaps during the Amazonian period (< 3 Ga). Other sulfate-bearing regions in the chaotic terrains may also contain small outcrops of ferric hydroxysulfate that have not yet been well characterized. Sowe et al.[36] observed a narrow band near 2.23 μm in Aureum Chaos (west of Aram Chaos) that they interpreted as a jarosite-like ferric sulfate phase and may actually be $Fe^{3+}SO_4OH$. This current study highlights the active nature of the martian surface, where geothermal processes altered hydrated materials more recently than formerly realized.

Methods

CRISM image analysis

CRISM images can be found at the Planetary Data System (PDS) Geosciences server under Mars Orbital Data Explorer: https://ode.rsl.wustl.edu/mars/. We used CRISM images FRT00005814, FRT000098B2, and HRL0000646A for this study. Mineral outcrops were investigated using advanced calibration versions[9] of these CRISM images that provide improved resolution of small outcrops and offer cleaner spectra that facilitate identifying specific minerals This algorithm includes simultaneous atmospheric correction and denoising of CRISM images in the 1.0–2.6 μm spectral range that removes most of the residual atmospheric bands and spurious noise[9].

We applied a recently developed algorithm that leverages the features learned by Generative Adversarial Networks (GAN) trained on hyperspectral data from CRISM[10]. This feature set has shown the ability to discriminate among different spectral shapes. CRISM maps of pyroxene, polyhydrated sulfates, monohydrated sulfates, $Fe^{3+}SO_4OH$, and a mixed phase containing a ~2.23 μm band and polyhydrated sulfate-type features were used to guide acquisition of spectra for minerals in the scene. Spectra were collected without ratioing the spectra of different spot sizes. For the thin polyhydrated sulfate and mixed

https://doi.org/10.1038/s41467-025-61801-2

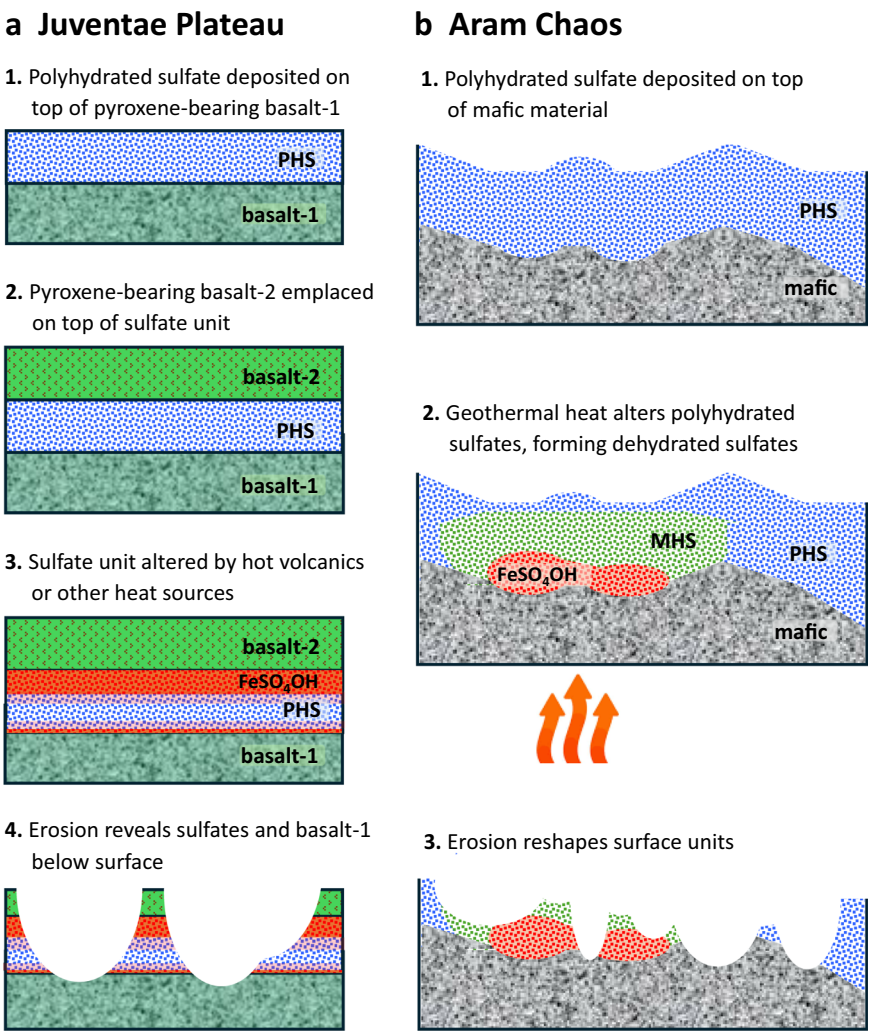

Fig. 7 | Diagrams illustrating potential formation models for $Fe^{3+}SO_4OH$. a This model outlines formation or deposition of polyhydrated sulfates on top of basaltic ash or lava, then emplacement of a different basaltic material on top of the sulfates. Heat from this upper basalt-2 unit then induces reaction of hydrous Fe^{2+} sulfates to partially alter to $Fe^{3+}SO_4OH$ at spatial scales of 20–50 m at the Juventae Plateau. Heat from the lower basalt-1 unit or another source heated the lower portion of the hydrous Fe^{2+} sulfates as well to form $Fe^{3+}SO_4OH$ in some places. **b** The second model begins similarly with formation or deposition of polyhydrated sulfates on top of a mafic unit at Aram Chaos, followed by geothermal heating of the region to form a combination of monohydrated sulfates and $Fe^{3+}SO_4OH$, where $Fe^{3+}SO_4OH$ forms at higher temperatures, closer to the heat source.

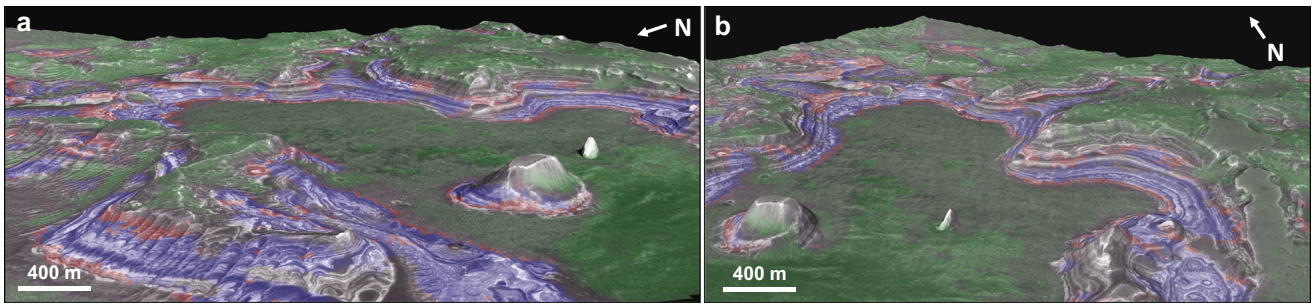

Fig. 8 | 3D views of sulfate-bearing regions on Juventae Plateau. a CRISM parameters over HiRISE with expanded view compared to Fig. 1c with 3x vertical exaggeration. Basalt-1 is shown in dark green, polyhydrated sulfate in blue, the $Fe^{3+}SO_4OH$-bearing phase in red, and basalt-2 in medium green. **b** Different view with same colors as (**a**).

polyhydrated sulfate/$Fe^{3+}SO_4OH$ units at the Juventae Plateau 3 × 3 pixel regions were used, while larger 5 × 5 and 10 × 10 pixel regions were used for the pyroxene outcrops at the Juventae Plateau and most regions at Aram Chaos. CRISM spectra collected in this way and used for this study are available in Supplementary data 1.

Blended views of CRISM, HiRISE, CTX, and HRSC imagery

CRISM mineral detections are merged with Context (CTX) and HRSC images over HRSC DTMs for regional stratigraphic views and over HiRISE images and DTMs for local stratigraphic views. ArcGIS software (ESRI) was used to overlay CRISM mineral maps over Mars

Reconnaissance Orbiter (MRO) HiRISE images at ~30 cm/pixel surface resolution[37] with coordinated mosaics of MRO CTX images at ~6 m/pixel surface resolution[38] and Mars Express HRSC images at ~10 m surface resolution[39,40]. The HRSC DTM has a grid size of 50 m and the HiRISE DTM has a grid size of 1 m. The HiRISE DTM was generated using methods developed by Kirk et al.[41] and McEwen et al.[42].

Lab experiments with hydrous ferrous sulfates

Synthesis of the rozenite[43] and szomolnokite[44] samples were loosely based on previous methods. Rozenite was formed by the dehydration of fine-grained $FeSO_4{\bullet}7H_2O$ reagent powder at room temperature (~22 °C) in a dry (i.e., 33% relative humidity) atmosphere maintained by a saturated $MgCl_2$ solution[45] in air over 7 days. Szomolnokite was obtained by dehydrating $FeSO_4{\bullet}7H_2O$ reagent powder over four days at 60 °C using the same humidity-buffer conditions. These samples are described in Table 1.

The phase identity and purity of the obtained sample materials and their heating products were confirmed by X-ray diffraction (Fig. 4, Supplementary Fig. S9). X-ray diffraction patterns were acquired on a Rigaku Smartlab diffractometer in Bragg-Brentano mode using Cu-K$\alpha_{1,2}$ radiation and D/teX Ultra 250 1D silicon strip detector. Diffraction patterns were acquired in the 5–65° 2θ range with a step size of 0.01° and a maximum scan speed of 1.5°/min. The instrument profile parameters were derived from a NIST 640c silicon standard and all Rietveld refinements were performed using GSAS-II[46]. The Rietveld refinements for the heating products of rozenite and szomolnokite are shown in Fig. 4.

Heating experiments were performed at temperatures of 50, 100, 200 °C for rozenite, and 100, 150, 200 and 250 °C for szomolnokite. The compositions of these samples are listed in Table 1.

Heating experiments in closed vials containing nitrogen gas and air

1.0 g of szomolnokite, synthesized and analyzed for phase purity following the workflow detailed above, were transferred into four individual vials of a volume of 155 ml. Three vials (two containing mineral, one empty control) were sparged with nitrogen gas for 2 min, whereas the other three contained ambient air as a top gas. The vials were then closed with a rubber stopper and sealed.

Using a Keller LEO2 manometer adapted to fit a 25 G disposable needle for insertion through the rubber stopper into vials, we observed a drop in pressure inside the vial during preliminary experiments, thus 50 ml of the respective top gas were injected into the vials using a 100 ml gas-tight Hamilton syringe before heating to end up with a pressure exceeding ambient atmospheric pressure. This allowed for gas sampling and analysis of O_2 composition at the end of the experiment. The vial pressures were measured before and after the heating cycle using the manometer. This was followed by the measurement of the oxygen concentration in the air vials on an SRI 8610C Gas Chromatographer (GC) equipped with a HaySepD column set to a temperature of 80 °C and a thermal conductivity detector. Nitrogen was used as the carrier gas with a flow rate of 29 ml/min. A quantification curve for oxygen was built by performing triplicate injections with 50 µl and 250 µl Hamilton gas-tight syringes fitted with removable 22 s gauge needles of 10, 25, 50, 100, and 250 µl volumes of a research-grade (99.999% purity) oxygen standard stored in a 155 ml serum bottle to emulate experimental conditions. This achieved standard concentrations of 4, 10, 20, 40 and 100% O_2 respectively. 250 µl of the experimental vial top gas was sampled in triplicate for analysis on the GC. The analytical error for this analysis is <1% and the experiment details are summarized in Supplementary S1/Supplementary Table 1.

The samples were heated on a hot plate by increasing the temperature by 50 °C every 10 min from 100 to 250 °C, followed by 20 min each at 280, 300 °C and 30 min at 320 °C. The same holding times and temperature steps were used when the hot plate temperature was decreased to 100 °C. Then the hot plate was turned off with the vials still on the hot plate for 10 min, after which they were removed to allow them to cool down to room temperature prior to measuring the vial pressure.

This was followed by another quantification of the oxygen-concentration in the air-filled vials using the workflow stated above. Lastly, all vials were opened, and the solid heating product was analyzed by means of X-ray diffraction on the Rigaku Smartlab diffractometer using the data acquisition parameters described in detail in the previous section.

Reflectance spectroscopy measurements of $Fe^{3+}SO_4OH$

SETI institute. Spectra were collected from 0.35 to 2.5 µm relative to Spectralon under ambient conditions using an Analytical Spectral Devices (ASD Inc; now part of Malvern Panalytical) FieldSpecPro FR instrument to check progress of the reactions in our experiments. The spectral resolution is 3 nm from 0.35 to 1.0 µm and 10 nm from 1.0 to 2.5 µm. Spectra were acquired with a contact probe on particulate samples in a black Teflon dish.

Reflectance Experiment Laboratory (RELAB) at Brown University. Spectra were measured under dry air with a diffuse gold standard from ~1 to 100 µm using a Thermo Nexus 870 FTIR instrument equipped with a tungsten-halogen lamp and a CaF_2 beam splitter (NIR), a globar source, a KBr beam splitter (MIR-FIR), and Deuterated TriGlycine-Sulfate (DTGS) detectors with spectral resolutions of 2 cm^{-1} (NIR) and 4 cm^{-1} (MIR-FIR) as in recent studies, e.g. ref. 47. The samples were placed in the sample chamber for ~12 h under N_2 in order to remove H_2O and CO_2 adsorbed on the surface of the grains or in the air above them, e.g. refs. 48,49. These data were scaled near 1.2 µm to bidirectional VNIR spectra recorded from 0.3 to 2.5 µm relative to Spectralon at 5 nm spectral sampling under ambient conditions as in previous studies, e.g. ref. 50. The spectrum of rozenite burnt by the FTIR beam was achieved using the globar source with an aperture size of 150 for 90 min. Only the upper few grains of the sample surface were affected. The change in spectral features of the rozenite sample including formation of bands consistent with szomolnokite occurred together with a darkening spot on the surface of the sample. Spectral measurements of rozenite samples with an aperture size of 55 or smaller did not change color or spectral properties. RELAB spectra of the samples discussed in this study are included in Supplementary data 2.

Institut de Planétologie et d'Astrophysique de Grenoble (IPAG) at the University of Grenoble Alpes (UGA). Spectra were measured from ~0.4 to 4.2 µm, relative to Spectralon below 1.3 µm and Infragold above that, using the SHINE bidirectional spectro-goniometer[51]. All spectra have been acquired with nadir illumination and an emission angle of 20°. Spectral sampling was 10 nm with a spectral resolution varying between 5 and 38 nm. Measurements were carried out within the CARBONIR environmental chamber under ~10^{-4} mbar vacuum at room temperature and under 12 mbar pure N_2 gas at lower temperatures down to 189 K at 30 K intervals, as in previous studies[52,53].

Planetary Spectroscopy Laboratory (PSL) at the German Aerospace Center (DLR) in Berlin. Spectra were measured from ~1 to 25 µm using a Bruker FTIR instrument under ~10^{-3} torr vacuum relative to a rough gold surface, as in previous studies[52].

Data availability

The CRISM, CTX, and HiRISE images used in this study are available on the Planetary Data System (PDS) Geosciences Node under "Mars Reconnaissance Orbiter" at https://ode.rsl.wustl.edu/mars/productsearch. The spectral data created for this study are provided as xls files as part of the supplementary information. Supplementary data 1 includes CRISM spectra of Mars shown in Supplementary Figs. S1–S3. Supplementary data 2 includes lab spectra of minerals and $Fe^{3+}SO_4OH$

used for comparison with the CRISM spectra. These data are also included at https://ahed.nasa.gov/datasets/b425b97a4c6d28c04f87d5b49f36. Additional mineral spectra are available at the RELAB spectral library (https://speclib.rsl.wustl.edu/search.aspx?catalog=RELAB) and the USGS spectral library (https://www.usgs.gov/labs/spectroscopy-lab/science/spectral-library).

References

1. Murchie, S. L. et al. in *Remote Compositional Analysis: Techniques for Understanding Spectroscopy, Mineralogy, and Geochemistry of Planetary Surfaces* (eds J. L.Bishop, J. E. Moersch, & J. F.Bell III) 453-483 (Cambridge University Press, 2019). https://doi.org/10.1017/9781316888872
2. Ehlmann, B. L. & Edwards, C. S. Mineralogy of the martian surface. *Annu. Rev. Earth Planet. Sci.* **42**, 291–315 (2014).
3. Squyres, S. W. et al. Overview of the opportunity Mars exploration rover mission to Meridiani Planum: Eagle crater to Purgatory Ripple. *J. Geophys. Res.* **111**, E12S12 (2006).
4. Rampe, E. B. et al. Mineralogy and geochemistry of sedimentary rocks and eolian sediments in Gale crater, Mars: a review after six Earth years of exploration with Curiosity. *Geochemistry* **80**, 125665 (2020).
5. Siljeström, S. et al. Evidence of sulfate-rich fluid alteration in Jezero Crater Floor, Mars. *J. Geophys. Res. Planets* **129**, e2023JE007989 (2024).
6. Bishop, J. L. et al. Mineralogy of Juventae Chasma: Sulfates in the light-toned mounds, mafic minerals in the bedrock, and hydrated silica and hydroxylated ferric sulfate on the plateau. *J. Geophys. Res.* **114**, E00D09 (2009).
7. Lichtenberg, K. A. et al. Stratigraphy of hydrated sulfates in the sedimentary deposits of Aram Chaos, Mars. *J. Geophys. Res.* **115**, E00D17 (2010).
8. Morris, R. V. et al. Visible and near-IR reflectance spectra for smectite, sulfate and perchlorate under dry conditions for interpretation of martian surface mineralogy. In *40th Lunar and Planetary Science Conference*, https://www.lpi.usra.edu/meetings/lpsc2009/pdf/2317.pdf (2009).
9. Itoh, Y. & Parente, M. A new method for atmospheric correction and de-noising of CRISM hyperspectral data. *Icarus* **354**, 114024 (2021).
10. Saranathan, A. M. & Parente, M. Adversarial feature learning for improved mineral mapping of CRISM data. *Icarus* **355**, 114107 (2021).
11. Wilk, K. A. et al. Characterization of aqueous alteration and formation of salty exposures at Ius Chasma, Mars. *icarus* **408**, 115800 (2024).
12. Bishop, J. L. et al. Characterizing the spectral properties of $FeSO_4OH$ - a new phase observed on Mars. In *55th Lunar Planetary Science Conference*, https://www.hou.usra.edu/meetings/lpsc2024/pdf/1880.pdf (2024).
13. Meusburger, J. M. et al. Ferric hydroxysulfate on Mars and its formation from ferrous sulfate hydrates. In *Tenth International Conference on Mars*, https://www.hou.usra.edu/meetings/tenthmars2024/pdf/3453.pdf (2024).
14. Bishop, J. L. in *Remote compositional analysis: techniques for understanding spectroscopy, mineralogy, and geochemistry of planetary surfaces* (eds, Bishop, J. L., Bell III, J. F., & Moersch, J. E.) 68–101 (Cambridge University Press, 2019). https://doi.org/10.1017/9781316888872.
15. Crowley, J. K. Visible and near-infrared (0.4–2.5 μm) reflectance spectra of Playa evaporite minerals. *J. Geophys. Res. Solid Earth* **96**, 16231–16240 (1991).
16. Cloutis, E. A. et al. Detection and discrimination of sulfate minerals using reflectance spectroscopy. *Icarus* **184**, 121–157 (2006).
17. Talla, D. & Wildner, M. Investigation of the kieserite–szomolnokite solid-solution series, (Mg,Fe)SO4·H2O, with relevance to Mars: Crystal chemistry, FTIR, and Raman spectroscopy under ambient and martian temperature conditions. *Am. Miner.* **104**, 1732–1749 (2019).
18. Bishop, J. L. & Murad, E. The visible and infrared spectral properties of jarosite and alunite. *Am. Miner.* **90**, 1100–1107 (2005).
19. Baur, W. H. Zur Kristallchemie der Salzhydrate. Die Kristallstrukturen von MgSO4.4H2O (Leonhardtit) und FeSO4.4H2O (Rozenit). *Acta Crystallogr.* **15**, 815–826 (1962).
20. Bishop, J. L., Yeşilbaş, M., Talla, D. & Hiroi, T. Spectral properties of dehydrated Fe hydroxy sulfates and implications for Mars. In *52nd Lunar and Planetary Science Conference*, https://www.hou.usra.edu/meetings/lpsc2021/pdf/1159.pdf (2021).
21. Ventruti, G. et al. High-temperature study of basic ferric sulfate, FeOHSO4. *Phys. Chem. Miner.* **47**, 43 (2020).
22. Yeşilbaş, M. et al. Low-temperature reflectance spectra of szomolnokite and applications for their detection on Mars. In *55th Lunar and Planetary Science Conference* https://www.hou.usra.edu/meetings/lpsc2024/pdf/2035.pdf (2024).
23. Mangold, N., Ansan, V., Masson, P., Quantin, C. & Neukum, G. Geomorphic study of the fluvial landforms on the northern Valles Marineris plateau, Mars. *J. Geophys. Res.* **113**, https://doi.org/10.1029/2007JE002985 (2008).
24. Weitz, C. M. et al. Light-toned strata and inverted channels adjacent to Juventae and Ganges Chasmata, Mars. *Geophys. Res. Lett.* **35**, L19202 (2008).
25. Mellon, M. T., Fergason, R. L. & Putzig, N. E. in *The martian surface: composition, mineralogy and physical properties Cambridge planetary science* (ed Jim, B.) 399–427 (Cambridge University Press, 2008).
26. Weitz, C. M. A marriage made on Mars: using HiRISE and CRISM data sets to study light-toned hydrated deposits in and around Valles Marineris. In *GSA Connects*. https://gsa.confex.com/gsa/2021AM/webprogram/Paper364841.html (2021).
27. Carr, M. H. Formation of martian flood featues by release of water from confined aquifers. *J. Geophys. Res.* **84**, 2995–3007 (1979).
28. Hartmann, W. K. & Neukum, G. Cratering chronology and the evolution of Mars. *Space Sci. Rev.* **96**, 165–194 (2001).
29. Glotch, T. D. & Christensen, P. R. Geologic and mineralogic mapping of Aram Chaos: evidence for a water-rich history. *J. Geophys. Res.* **110**, E09006 (2005).
30. Rodriguez, J. A. P. et al. Outflow channel sources, reactivation, and chaos formation, Xanthe Terra, Mars. *Icarus* **175**, 36–57 (2005).
31. Wildner, M. & Giester, G. The crystal structure of kieserite-type compounds. I. Crystal structures of Me(II)SO4•H2O (Me = Mn, Fe, Co, Ni, Zn). *Neues Jahrb. für Mineralogie Monatshefte* **1991**, 296–306 (1991).
32. Lu, Y. & Wang, A. in *43rd Lunar Planetary Science Conference* (The Woodlands, TX, 2012).
33. Massé, M. et al. Mineralogical composition, structure, morphology, and geological history of Aram Chaos crater fill on Mars derived from OMEGA Mars Express data. *J. Geophys. Res.* **113**, https://doi.org/10.1029/2008JE003131 (2008).
34. Scott, D. H. & Tanaka, K. L. Geologic map of the western equatorial region of Mars, USGS Misc., Invest. Ser. Map I-1802-A, 1:15000000 scale (U.S. Geol. Surv., Reston, VA, 1986).
35. Chapman, M. G., Gudmundsson, M. T., Russell, A. J. & Hare, T. M. Possible Juventae Chasma subice volcanic eruptions and Maja Valles ice outburst floods on Mars: Implications of Mars Global Surveyor crater densities, geomorpholoy, and topography. *J. Geophys. Res.* **108**, https://doi.org/10.1029/2002JE002009 (2003).
36. Sowe, M., Wendt, L., McGuire, P. C. & Neukum, G. Hydrated minerals in the deposits of Aureum Chaos. *Icarus* **218**, 406–419 (2012).
37. McEwen, A. S. et al. Mars reconnaissance orbiter's high resolution imaging science experiment (HiRISE). *J. Geophys. Res.* **112**, E05S02 (2007).

38. Malin, M. C. et al. Context camera investigation on board the Mars reconnaissance orbiter. *J. Geophys. Res.* **112**, E05S04 (2007).
39. Neukum, G. et al. Recent and episodic volcanic and glacial activity on Mars revealed by the high resolution stereo camera. *Nature* **432**, 971–979 (2004).
40. Gwinner, K. et al. The high resolution stereo camera (HRSC) of Mars express and its approach to science analysis and mapping for Mars and its satellites. *Planet. Space Sci.* **126**, 93–138 (2016).
41. Kirk, R. L. et al. Ultrahigh resolution topographic mapping of Mars with MRO HiRISE stereo images: meter-scale slopes of candidate Phoenix landing sites. *J. Geophys. Res.* **113**, E00A24 (2008).
42. McEwen, A. S. et al. The High Resolution Imaging Science Experiment (HiRISE) during MRO's Primary Science Phase (PSP). *Icarus* **205**, 2–37 (2010).
43. Meusburger, J. M. et al. Low-temperature crystallography and vibrational properties of rozenite (FeSO4·4H2O), a candidate mineral component of the polyhydrated sulfate deposits on Mars. *Am. Miner.* **108**, 1080–1091 (2023).
44. Chio, C. H., Sharma, S. K. & Muenow, D. W. The hydrates and deuterates of ferrous sulfate (FeSO4): a Raman spectroscopic study. *J. Raman Spectrosc.* **38**, 87–99 (2007).
45. Greenspan, L. Humidity fixed points of binary saturated aqueous solutions. *J. Res. Natl Bur. Stand.* **81A**, 89–96 (1977).
46. Toby, B. H. & Von Dreele, R. B. GSAS-II: the genesis of a modern open-source all purpose crystallography software package. *J. Appl. Crystallogr.* **46**, 544–549 (2013).
47. Milliken, R. E., Hiroi, T. & Patterson, W. R. The NASA Reflectance Experiment Laboratory (RELAB) facility: past, present, and future. In *48th Lunar Planet. Science Conf.* https://www.hou.usra.edu/meetings/lpsc2016/pdf/2058.pdf (2016).
48. Bishop, J. L., Dyar, M. D., Lane, M. D. & Banfield, J. F. Spectral identification of hydrated sulfates on Mars and comparison with acidic environments on Earth. *Int. J. Astro* **3**, 275–285 (2004).
49. Bishop, J. L. et al. Spectral properties of Ca-sulfates: Gypsum, bassanite and anhydrite. *Am. Miner.* **99**, 2105–2115 (2014).
50. Pieters, C. M. & Hiroi, T. RELAB (Reflectance Experiment Laboratory): A NASA multiuser spectroscopy facility. In *35th Lunar Planetary Science Conference*, https://www.lpi.usra.edu/meetings/lpsc2004/pdf/1720.pdf (2004).
51. Brissaud, O. et al. Spectrogonio radiometer for the study of the bidirectional reflectance and polarization functions of planetary surfaces. 1. Design and tests. *Appl. Opt.* **43**, 1926–1937 (2004).
52. Beck, P. et al. What is controlling the reflectance spectra (0.35–150 μm) of hydrated (and dehydrated) carbonaceous chondrites?. *Icarus* **313**, 124–138 (2018).
53. De Angelis, S. et al. Temperature-dependent VNIR spectroscopy of hydrated Mg-sulfates. *Icarus* **281**, 444–458 (2017).

Acknowledgements

The authors are grateful to the CRISM, HiRISE, CTX, and HRSC teams for collecting and archiving the images used in this study, the Planetary Spectroscopy Laboratory (PSL) at the DLR-Berlin, the Institut de Planétologie et d'Astrophysique de Grenoble (IPAG) at UGA and to G. Alemanno, O. Poch, and K. Wilk for assistance with the spectral measurements, and to T. Hoehler and M. Kubo for providing lab space, resources, and assistance with the GC measurements. Support from NASA SSW grant #80NSSC23K0032 (J.L.B., M.R.D.G., T.F.B., B.L.), NASA MDAP grants #80NSSC21K1103 (J.L.B., C.M.W., M.P., A.M.S., Y.I., M.R.D.G.) and 80NSSC23K1074 (C.M.W., J.L.B.), Austrian Science Fund (FWF) project #P34227-N (D.T., M.W.), Swedish Research Council project (V.R.) 2021-05859 (M.Y.), NASA postdoctoral program fellowships (J.M.M., A.E.G.H.), and the EU Europlanet TA program (J.L.B., M.Y., B.S., A.M.) are greatly appreciated. Europlanet 2024 RI has received funding from the European Union's Horizon 2020 research and innovation programme under grant agreement No 871149. RELAB is a multiuser facility supported by the NASA PSEF program (T.H.). The Open Planetary Science Initiative and AHED thank NASA's Planetary Sciences Division for its continued support (T.F.B., B.L.).

Author contributions

Author roles: J.L.B. conceived of the study, conducted a large part of the analyses, prepared most figures, and wrote most of the text. J.M.M. prepared most samples, conducted most XRD analyses, created some figures, and wrote part of the text. D.T. prepared some samples and participated in sample analysis. A.E.G.H. led the reactions under controlled environments. J.L.B., M.Y., T.F.B. & B.L. contributed to initial heating experiments and sample analysis. M.W. assisted with sample synthesis, sample analysis, and figure preparation. T.H. measured reflectance spectra of all samples at RELAB. M.Y. & B.S. conducted the low-temperature VNIR experiments. A.M. & J.L.B. conducted the vacuum FTIR measurement. M.P., A.M.S. & Y.I. prepared the improved CRISM images and constructed the mineral maps. M.R.D.G. & J.L.B. analyzed the CRISM images, collected CRISM spectra and compared them to spectra of minerals. C.M.W. analyzed the HiRISE images, prepared blended CRISM-HiRISE views and wrote part of the text. C.G. analyzed the HRSC images and prepared the blended CRISM-HRSC views. J.L.B., M.A. & C.M.W. developed the formation models. All authors provided comments and/or revisions to the paper.

Competing interests

The authors declare no competing interests.

Additional information

Supplementary information The online version contains supplementary material available at https://doi.org/10.1038/s41467-025-61801-2.

Correspondence and requests for materials should be addressed to J. L. Bishop.

Peer review information *Nature Communications* thanks Kathleen Benison, Megan Elwood Madden and Clément Royer for their contribution to the peer review of this work. A peer review file is available.